# NMR Quantum Simulation of Localization Effects Induced by Decoherence

Gonzalo A. Álvarez* and Dieter Suter†

*Fakultät Physik, Universität Dortmund, Otto-Hahn-Strasse 4, D-44221 Dortmund, Germany*

(Received 21 January 2010; published 9 June 2010)

The loss of coherence in quantum mechanical superposition states limits the time for which quantum information remains useful. Similarly, it limits the distance over which quantum information can be transmitted. Here, we investigate in a nuclear spin-based quantum simulator, the localization of the size of spin clusters that are generated by a Hamiltonian driving the transmission of information, while a variable-strength perturbation counteracts the spreading. We find that the system reaches a dynamic equilibrium size, which decreases with the square of the perturbation strength.

DOI: 10.1103/PhysRevLett.104.230403 PACS numbers: 03.65.Yz, 03.67.Ac, 72.15.Rn, 76.60.−k

*Introduction.*—Quantum information processing has the potential of solving computational problems for which no efficient solution exists on classical computers [1]. Transfer and exchange of quantum information and quantum entanglement can be used for secure transmission of information [2,3]. Realization of this potential for practical applications requires precise control of large quantum registers. However, as the number of qubits increases, the quantum mechanical superposition states of the system become more fragile [4]. This degradation of quantum superpositions, called decoherence [5], is due to extra degrees of freedom (the environment) that interact with the system, and to imperfections of the gate operations. Overcoming decoherence is clearly one of the key factors for implementing large scale quantum computers. Several techniques have been proposed for this purpose, including dynamical decoupling [6], decoherence-free subspaces [7], and quantum error correction [8,9]. These proposals have been tested on small systems of nuclear spins [10], trapped ions [11], or spin model quantum memories [12].

Tests on larger systems, comprising hundreds or thousands of qubits, are more difficult. So far, the only physical system that offered this possibility is nuclear magnetic resonance (NMR) of dipolar coupled spins [4,13]. Processes that transfer quantum information over large distances can also be studied in spin chains [3]. An example of such a linear spin system was studied by solid-state NMR [14]. These model systems do not allow addressing of individual qubits, but they allow one to study some aspects of decoherence and information transfer. In particular, they can be used for studying the effect of the finite precision of experimental quantum gate operations on the transfer of quantum states: it was predicted that quantum information cannot be transmitted over arbitrary distances, but that it will become localized [15,16].

In this Letter, we present the first experimental study trying to answer the following question: How far can quantum information be transmitted with quantum gate operations of finite precision? For this purpose, we use a NMR quantum simulator. Starting from individual, uncorrelated spins, we measure the buildup of clusters of correlated spins of increasing size. Introducing a perturbation to the Hamiltonian that generates these clusters, we find that the size of the clusters reaches an upper bound. This upper bound appears to be a dynamic equilibrium: if the cluster size is initially larger than this equilibrium value, it decreases under the effect of the perturbed Hamiltonian, while the unperturbed Hamiltonian leads to an increase. The equilibrium size decreases with increasing strength of the perturbation.

*Growth of spin clusters.*—All the spins of the system are equivalent and they are in a strong magnetic field. In its Zeeman rotating frame, the Hamiltonian of the spin system used for the quantum simulations is the high-field homonuclear dipolar interaction [17]

$$\hat{\mathcal{H}}_{dd} = \sum_{i<j} d_{ij}[2\hat{I}_z^i\hat{I}_z^j - (\hat{I}_x^i\hat{I}_x^j + \hat{I}_y^i\hat{I}_y^j)], \tag{1}$$

where $\hat{I}_x^i$, $\hat{I}_y^i$, and $\hat{I}_z^i$ are spin-1/2 operators and $d_{ij}$ the coupling constants. The quantum simulations start from the high-temperature thermal equilibrium [17], $\hat{\rho}_0 \propto \hat{I}_z = \sum \hat{I}_z^i$. In this state, the spins are uncorrelated.

We generate states with correlated spin clusters whose density operator terms are of the form $\hat{I}_u^i \ldots \hat{I}_v^j \hat{I}_w^k$ ($u, v, w = x, y, z$), by letting the system evolve under the effective Hamiltonian

$$\hat{\mathcal{H}}_0 = -\sum_{i<j} d_{ij}[\hat{I}_x^i\hat{I}_x^j - \hat{I}_y^i\hat{I}_y^j]. \tag{2}$$

This Hamiltonian is prepared by means of a standard NMR sequence [18,19] shown in the upper part of Fig. 1. This Hamiltonian flips simultaneously two spins with the same orientation. Accordingly, the $z$ component of the magnetization $M_z$ changes by $M = \Delta M_z = \pm 2$. At the same time, the number $K$ of correlated spins changes by $\Delta K = \pm 1$.

To determine the average number of correlated spins, we use standard NMR techniques developed by Baum *et al.* [19]. The technique relies on the fact that in a system of $K$ spins, the number of transitions with a given $M$ shows a

 

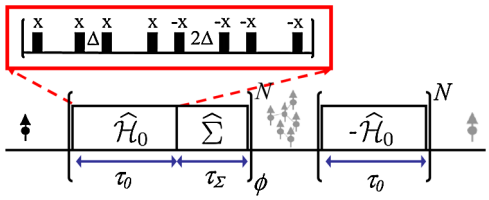


FIG. 1 (color online). NMR sequence for the quantum simulations. An unperturbed evolution is achieved when $\tau_\Sigma = 0$. The effective Hamiltonian $\hat{\mathcal{H}}_0$ is generated by the sequence of $\pi/2$ pulses shown in the upper part of the figure.

binomial distribution. For $K \gg 1$, the binomial distribution can be well approximated with a Gaussian of width $\propto \sqrt{K}$. To determine the effective size of the spin clusters in a given state, we decompose its density operator $\rho$ into components of coherence order $M$. They can be distinguished experimentally by rotating the system around the $z$ axis: a rotation $\hat{\phi}_z = e^{-i\phi\hat{I}_z}$ by $\phi$ changes the density operator to

$$\hat{\rho}(\phi) = \hat{\phi}_z \hat{\rho} \hat{\phi}_z^{-1} = \sum_M \hat{\rho}_M e^{iM\phi}, \tag{3}$$

where $\hat{\rho}_M$ contains all the elements of the density operator involving coherences of order $M$. The terms with $M = 0$ are zero quantum coherences and populations.

If the system evolves under the Hamiltonian (2), the cluster size increases indefinitely, as shown in Fig. 2. The figure also shows two examples of $\hat{\rho}_M$ distributions.

This evolution can be reversed completely by changing the Hamiltonian from $\hat{\mathcal{H}}_0$ to $-\hat{\mathcal{H}}_0$. Experimentally, this is achieved by shifting the phase of all rf pulses by $\pm\pi/2$ [18]. This indefinite growth of the cluster size, as well as the reversibility of the time evolution, is no longer possible

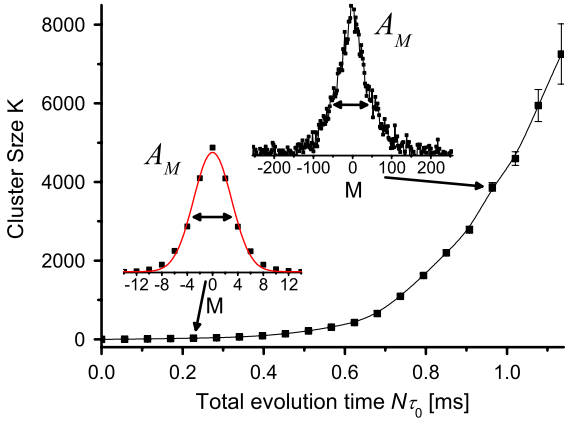


FIG. 2 (color online). Time evolution of the cluster size of correlated spins with the unperturbed Hamiltonian $\hat{\mathcal{H}}_0$. Distributions of the squared amplitudes $A_M$ of density operator components as a function of the coherence order $M$ are shown for two different cluster sizes. The latter are obtained from the half-width $2\sqrt{\ln(2K)}$ of the distribution function $A_M$.

if the effective Hamiltonian deviates from the ideal form (2). This allows us to experimentally induce localization effects by concatenating short evolution periods under a perturbation Hamiltonian $\hat{\Sigma}$ with evolution periods under the ideal Hamiltonian $\hat{\mathcal{H}}_0$. For the present experiments, we choose $\hat{\Sigma} = \hat{\mathcal{H}}_{dd}$, and we label the durations of the two time periods $\tau_\Sigma$ and $\tau_0$, as shown in Fig. 1. When the duration $\tau_c = \tau_0 + \tau_\Sigma$ of each cycle is short compared to the inverse of the dipolar couplings $d_{ij}$, the resulting evolution can be described by the effective Hamiltonian

$$\hat{\mathcal{H}}_{\text{eff}} = (1-p)\hat{\mathcal{H}}_0 + p\hat{\Sigma}, \tag{4}$$

where the relative strength $p = \tau_\Sigma/\tau_c$ of the perturbation can be controlled by adjusting the duration $\tau_\Sigma$. Since the Hamiltonian $\hat{\mathcal{H}}_0$ is generated as an effective Hamiltonian, it always deviates from the ideal Hamiltonian. In the experiment, we compare the artificially perturbed evolution of $\hat{\mathcal{H}}_{\text{eff}}$ with the $\hat{\mathcal{H}}_0$ evolution with its intrinsic errors. Note that the intrinsic errors do not produce localization on the time scale of our experiments (see Fig. 2).

Taking this perturbation into account, and starting from thermal equilibrium, the state of the system at the end of $N$ cycles is

$$\hat{\rho}^{\mathcal{H}_{\text{eff}}}(N\tau_c) = \hat{U}_N^\dagger \hat{I}_z \hat{U}_N, \tag{5}$$

where $\hat{U}_N = \exp\{-\frac{i}{\hbar}\hat{\mathcal{H}}_{\text{eff}} N\tau_c\}$ is the evolution operator for the perturbed evolution. The NMR signal, which is measured after the backward evolution $\hat{V}_N = \exp\{\frac{i}{\hbar}\hat{\mathcal{H}}_0 N\tau_0\}$, can be written as $S(N\tau_c) = \text{Tr}\{\hat{\mathcal{A}}\hat{\rho}^{\mathcal{H}_{\text{eff}}}(N\tau_c)\}$, where

$$\hat{\mathcal{A}} = \hat{V}_N \hat{I}_z \hat{V}_N^\dagger = \hat{\rho}^{\mathcal{H}_0}(N\tau_0) \tag{6}$$

is the effective observable and $\hat{\rho}^{\mathcal{H}_0}$ the density operator of the unperturbed evolution. We again determine the cluster size by applying rotations $\hat{\phi}_z$ around the $z$ axis, as in Eq. (3). The resulting NMR signal is then

$$\begin{aligned} S(\phi, N\tau_c) &= \sum_M e^{i\phi M} A_M \\ &= \sum_M e^{i\phi M}\,\text{Tr}\{\hat{\rho}_M^{\mathcal{H}_0}(N\tau_0)\hat{\rho}_M^{\mathcal{H}_{\text{eff}}}(N\tau_c)\}. \end{aligned} \tag{7}$$

For ideal evolution ($p = 0$), the individual terms $A_M$ in the last equation correspond to the squared amplitudes of density operator elements $\hat{\rho}_M^{\mathcal{H}_0}(N\tau_0)$ with coherence order $M$. For perturbed evolution ($p \neq 0$), they are reduced by the overlap of the actual density operator elements $\hat{\rho}_M^{\mathcal{H}_{\text{eff}}}(N\tau_c)$ with the ideal ones. To extract these amplitudes from the experimental data, we perform a Fourier transform with respect to $\phi$. Two examples for the resulting $A_M$ are shown in the insets of Fig. 2.

*Experimental results.*—Experiments were performed on a homebuilt solid-state NMR spectrometer with a $^1$H resonance frequency of 300 MHz. The spins are the protons of polycrystalline adamantane where the strength of the dipolar interaction, quantified by the second moment of the resonance line, is 7.9 kHz. In the experiments we chose $\tau_0 = 57.6\ \mu$s. The black squares of Fig. 3(a) show the averaged number of correlated spins as a function of time for an unperturbed evolution, $p = 0$. The observed cluster size $K(N\tau_c)$ grows almost exponentially over the range considered here [20]. The other symbols of 3(a) show the evolution of the number of correlated spins for different values of $p$. Initially, the cluster size $K(N\tau_c)$ starts to grow as in the unperturbed evolution, but then it saturates after a time that decreases with increasing perturbation strength $p$. We consider this as evidence of localization due to the perturbation. The size of the cluster at which this saturation occurs is also determined by the strength of the perturbation: increasing perturbation strength reduces the limiting cluster size. Figures 3(b) and 3(c) visualize this localization directly by comparing the generation of high-order multiple quantum coherences for unperturbed [3(b)] and perturbed [3(c), $p = 0.108$] evolution: they give a color-coded representation of the amplitudes $A_M(N\tau_c)$ as a function of evolution time $N\tau_c$. While the distribution spreads continuously in 3(b), it reaches a limiting value in 3(c).

While these experiments show that the cluster size reaches a stationary value, they leave open the question of whether this limiting size results from a slow down in the growth [16] or if it represents a dynamic equilibrium state. We therefore repeated the above experiment for a series of initial conditions corresponding to different clusters sizes. Figure 4(a) shows the corresponding pulse sequence: The initial state preparation, consisting of an evolution of duration $N_0\tau_0$ under the unperturbed Hamiltonian $\hat{\mathcal{H}}_0$, generates clusters of size $K_0$. During the subsequent perturbed evolution of duration $N\tau_c$, these initial clusters grow or shrink. Figure 4(b) shows the results for two perturbation strengths, $p = 0.034$ and $p = 0.065$. The filled symbols correspond to uncorrelated initial states and the empty symbols to various initial cluster sizes $K_0$. The experimental results clearly show that, for a given perturbation strength, the size of the spin clusters tends towards the same limiting value, independent of the initial condition. We verified this behavior for additional perturbation strengths (data not shown in the figure).

Figures 3(a) and 4(b) indicate that the size of the resulting clusters decreases with increasing strength of the perturbation. To establish this dependence in a quantitative manner, we determined the size of the localized clusters from the data shown in Fig. 3 and plotted them against the perturbation strength (black squares in Fig. 5). The diagonal line in Fig. 5 represents a linear fit to the experimental data represented by the black squares; its width indicates the error of the fit. A functional dependence $K_{\mathrm{loc}} \sim p^{-1.86\pm0.05}$ is obtained, indicating that the size of the localized clusters decreases with the square of the perturbation strength. The limiting value for $p = 1$ is $K_{\mathrm{loc}} \approx 1$, indicating that the system becomes completely localized if the perturbation strength is significantly larger than the

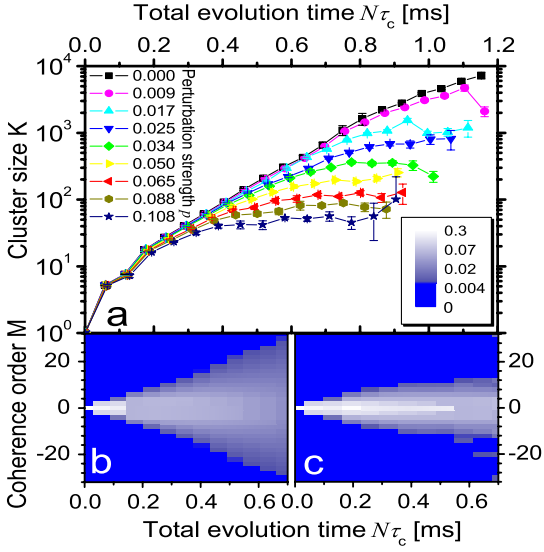


FIG. 3 (color online). (a) Time evolution of the cluster size. The black squares represent the unperturbed time evolution and the other symbols correspond to different perturbation strengths according to the legend. (b),(c) Distributions of the amplitudes $A_M(N\tau_c)$ for unperturbed dynamics [(b), $p = 0$] and a perturbed evolution [(c), $p = 0.108$], respectively. The perturbed evolution in (c) shows localization at a cluster size $K_{\mathrm{loc}} \simeq 56$ spins.

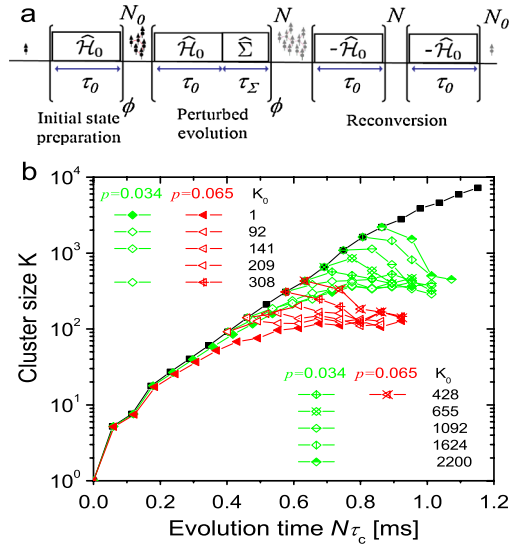


FIG. 4 (color online). (a) NMR pulse sequence for preparing different initial cluster sizes and subsequently evolving them in the presence of a perturbation. (b) Time evolution of the correlated cluster size starting from different initial sates. Filled symbols are evolutions from an uncorrelated initial state for two different perturbation strengths given in the legend. Empty symbols start from an initial state with $K_0$ correlated spins.

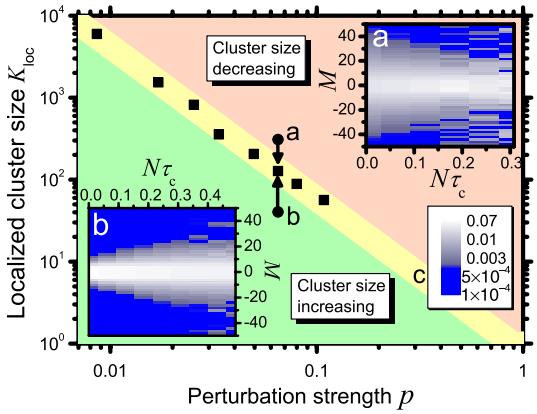


FIG. 5 (color online). Localized cluster size $K_{loc}$ (square symbols) of correlated spins versus the perturbation strength $p$. Three dynamical regimes for the evolution of the cluster size are identified depending on the number of correlated spins compared with the perturbation dependent localization value: (a) a cluster size decreases, (b) a cluster size increases, (c) stationary regime.

unperturbed Hamiltonian. The figure also summarizes the evolution of the cluster size before the static (localized) size is reached: If the initial size is larger than the stationary value for the given perturbation strength, $K_0 > K_{loc}$, the cluster shrinks [inset (a) in Fig. 5, above the diagonal]. If it is smaller, $K_0 < K_{loc}$, the size increases [inset (b) in Fig. 5, below the diagonal].

*Discussion and conclusions.*—Decoherence has long been recognized to limit the time for which quantum information can be used. Here, we have shown that it also limits the distance over which quantum information can be transferred. To demonstrate this effect, we have compared the spreading of information in a system of nuclear spins under the influence of a Hamiltonian that transfers information and a perturbation Hamiltonian of variable strength. In combination, these opposing forces result in a quantum state that becomes localized. The localization size decreases with increasing strength of the perturbation. Our experimental result of a dynamic equilibrium size of the localized state differs from theoretical predictions that only indicate a slow down of the spreading [16]. The experiments were performed with nuclear spins, which we use as a quantum simulator, and the perturbation is taken as a model for the disorder considered in the discussion of localization [15,16].

These results may also be connected to our earlier findings that the decoherence rate of quantum states with many correlated qubits increases with the size of the system [4], indicating that larger systems are more sensitive to perturbations. As the system size increases, the tendency for the system to spread is therefore balanced by the restriction due to the perturbation. As a heuristic argument, we note that in a suitable interaction representation, the perturbation will cause a decay whose rate may be calculated by second order perturbation theory. We expect there a quadratic dependence on the perturbation strength that could be the source of the dynamic equilibrium size behavior. The results presented here provide information about the spatial bounds for transferring quantum information in a spin network and indicate how precise manipulations of large quantum systems have to be.

G. A. A. thanks the Humboldt Foundation for financial support. We thank M. Lovric, H. G. Krojanski, and I. Niemeyer for helpful discussions and technical support.

*galvarez@e3.physik.uni-dortmund.de
†Dieter.Suter@tu-dortmund.de

[1] P. W. Shor, in *Proceedings of the 35th Annual Symposium on the Foundations of Computer Science*, edited by S. Goldwasser (IEEE Computer Society, Los Alamitos, 1994); D. P. DiVincenzo, Science **270**, 255 (1995); M. A. Nielsen and I. L. Chuang, *Quantum Computation and Quantum Information* (Cambridge University Press, Cambridge, England, 2000).
[2] J. I. Cirac *et al.*, Phys. Rev. Lett. **78**, 3221 (1997); M. Paternostro, H. McAneney, and M. S. Kim, *ibid.* **94**, 070501 (2005); D. Yang and J. Eisert, *ibid.* **103**, 220501 (2009).
[3] S. Bose, Phys. Rev. Lett. **91**, 207901 (2003).
[4] H. G. Krojanski and D. Suter, Phys. Rev. Lett. **93**, 090501 (2004).
[5] W. H. Zurek, Rev. Mod. Phys. **75**, 715 (2003).
[6] L. Viola, E. Knill, and S. Lloyd, Phys. Rev. Lett. **82**, 2417 (1999).
[7] D. A. Lidar, I. L. Chuang, and K. B. Whaley, Phys. Rev. Lett. **81**, 2594 (1998).
[8] J. Preskill, Proc. R. Soc. A **454**, 385 (1998).
[9] E. Knill, Nature (London) **434**, 39 (2005).
[10] E. M. Fortunato, *et al.*, Phys. Rev. A **67**, 062303 (2003).
[11] T. Monz *et al.*, Phys. Rev. Lett. **103**, 200503 (2009).
[12] M. J. Biercuk *et al.*, Nature (London) **458**, 996 (2009).
[13] H. G. Krojanski and D. Suter, Phys. Rev. Lett. **97**, 150503 (2006); M. Lovric, H. Krojanski, and D. Suter, Phys. Rev. A **75**, 042305 (2007).
[14] P. Cappellaro, C. Ramanathan, and D. Cory, Phys. Rev. A **76**, 032317 (2007); E. Rufeil-Fiori *et al.*, *ibid.* **79**, 032324 (2009).
[15] P. W. Anderson, Phys. Rev. **109**, 1492 (1958); A. Pomeransky and D. Shepelyansky, Phys. Rev. A **69**, 014302 (2004); J. Keating *et al.*, *ibid.* **76**, 012315 (2007); J. Allcock and N. Linden, Phys. Rev. Lett. **102**, 110501 (2009).
[16] C. K. Burrell and T. J. Osborne, Phys. Rev. Lett. **99**, 167201 (2007).
[17] C. P. Slichter, *Principles of Magnetic Resonance* (Springer-Verlag, Berlin, 1992), 2nd ed.
[18] W. Warren *et al.*, Phys. Rev. Lett. **43**, 1791 (1979).
[19] J. Baum *et al.*, J. Chem. Phys. **83**, 2015 (1985); J. Baum and A. Pines, J. Am. Chem. Soc. **108**, 7447 (1986).
[20] S. Lacelle, Adv. Magn. Opt. Reson. **16**, 173 (1991); V. Zobov and A. Lundin, JETP **103**, 904 (2006).